Expansion microsopy reveals *Plasmodium falciparum* blood-stage parasites undergo anaphase with a chromatin bridge in the absence of mini-chromosome maintenance complex binding protein.

Benjamin Liffner[1], Sabrina Absalon[1*]

[1]Department of Pharmacology and Toxicology, Indiana University School of Medicine, Indianapolis, IN, USA.

* Corresponding author

E-mail: Sabsalon@iu.edu

ABSTRACT

Mitosis in the malaria parasite *Plasmodium falciparum* undergoes closed mitosis, which occurs within an intact nuclear envelope, and differs significantly from its human host. Mitosis is underpinned by the dynamics of microtubules and the nuclear envelope. To date, our ability to study *P. falciparum* mitosis by microscopy has been hindered by the small size of *P. falciparum* nuclei. Ultrastructure expansion microscopy (U-ExM) has recently been developed for *P. falciparum*, allowing visualization of mitosis at the individual nucleus level. Using U-ExM, three intranuclear microtubule structures are observed: hemispindles, mitotic spindles and interpolar spindles. A previous study demonstrated that the mini-chromosome maintenance complex binding-protein (MCMBP) depletion caused abnormal nuclear morphology and microtubule defects. To investigate the role of microtubules following MCMBP depletion and study the nuclear envelope in these parasites, we developed the first nuclear stain enabled by U-ExM in *P. falciparum.* MCMBP deficient parasites show aberrant hemispindles and mitotic spindles. Moreover, anaphase chromatin bridges, and individual nuclei containing multiple microtubule structures were observed following MCMBP knockdown. Collectively, this study refines our model for the phenotype of MCMBP-deficient parasites and highlights the utility of U-ExM coupled with a nuclear envelope stain for studying mitosis in *P. falciparum*.

30 INTRODUCTION

31 Malaria is estimated cause over 400,000 deaths annually, these deaths are
32 predominantly in young children and are caused by the unicellular protozoan pathogen
33 *Plasmodium falciparum* [1]. Resistance against frontline antimalarials has emerged in many
34 parts of the globe and is spreading [2-6]. Moreover, there is no highly effective vaccine against
35 malaria, highlighting the need to develop new therapeutic interventions for ongoing and future
36 control of this disease. One therapeutic strategy is drug inhibition of DNA/RNA replication,
37 and/or cell division, a method that is commonly used for control of bacterial [7] and viral
38 diseases [8], along with many types of cancer [9]. The distinctive division method of *P.*
39 *falciparum* compared to its human host makes this an attractive strategy for *P. falciparum* drug
40 design, yet no current antimalarials directly target DNA replication or cell division [10];
41 highlighting the need for further investigation into this pathway.

42 *Plasmodium* parasites undergo cell division by a process known as schizogony, whereby
43 a singly nucleated parasite undergoes repeated rounds of DNA replication and mitosis, within
44 a shared cytoplasm, followed by a single cytokinetic event that results in the formation of 16-
45 32 daughter parasites [11-13]. Throughout division, *Plasmodium* undergoes closed mitosis,
46 where the nuclear envelope remains intact, as opposed to the open mitosis of its human host
47 [14]. Nuclear division during schizogony is orchestrated by a set of intranuclear microtubule
48 structures, which appear to be unique to *Plasmodium* [15,16]. The first observed microtubule
49 structure during the blood-stage of the lifecycle is the hemispindle, a collection of ~5
50 microtubule branches that extend from a single microtubule organizing center (MTOC)
51 throughout the nucleus [15-17]. It has been shown that around when DNA replication begins,
52 the hemispindle retracts, the MTOC duplicates, and the mitotic spindle is formed. Mitotic
53 spindles consist of short microtubules that extend from two opposing MTOCs and connect to
54 the kinetochore, in preparation for chromatid separation into daughter nuclei [15,16,18-21].

55 Following chromatid separation, two distinct and distant DNA masses are observed, each
56 containing their own MTOC, but connected by extended microtubules that are attached to both
57 MTOCs [16]. The nomenclature around this microtubule structure is inconsistent, but in this
58 study, they will be referred to as interpolar spindles. Following nuclear segregation, the
59 interpolar spindle retracts and the two daughter nuclei undergo nuclei fission before reforming
60 the hemispindle [16].

61 Mitosis in *Plasmodium* has been poorly studied historically. This is due to the small size
62 of *P. falciparum* nuclei (~1 µm diameter), which largely prevents visualization of events
63 occurring at a single-nucleus level by conventional microscopy techniques. Technological
64 advancements that overcome the resolution hurdle, along with recent work on other organisms
65 that undergo closed mitosis, have reignited interest in closed mitosis broadly and of
66 *Plasmodium* mitosis specifically. The application of Ultrastructural-expansion microscopy (U-
67 ExM), a sample preparation method that isotropically expands the sample ~4.5x, to *P.*
68 *falciparum* [22] has radically enhanced our ability to study the biology occurring inside
69 individual nuclei. Indeed U-ExM has already been used to observe microtubules in asexual
70 blood-stages, ookinetes and gametocytes [16,22,23]. Moreover, U-ExM has been used to
71 differentiate the intranuclear microtubules of *P.* falciparum, providing significance insight into
72 the physiology of microtubule dynamics in the process [16,22]. Outside of *Plasmodium*, a
73 recent study on the genetically tractable and much larger fission yeast that undergoes closed
74 mitosis, *Schizosaccharamyces pombe*, provided mechanistic insight into this fascinating
75 process, with a particular focus on the relationship between closed mitosis and nuclear
76 envelope dynamics [24]. With the application of U-ExM to *P. falciparum*, we can now begin
77 to study the closed mitosis of *Plasmodium* with a resolving power similar to fission yeast, the
78 most well studied model organism for closed mitosis. Notably, however, the absence of a

79 uniform marker for the nuclear envelope in *Plasmodium* largely precludes understanding of the
80 role of the nuclear envelope in closed mitosis.

81 Studies on *Plasmodium* microtubules historically have been largely descriptive and
82 relatively few individual proteins are known to influence microtubule dynamics. One protein
83 that has previously been shown to be involved in *P. falciparum* microtubule organization is the
84 mini-chromosome maintenance binding protein (MCMBP) [25]. In other organisms, MCMBP
85 is directly involved in DNA replication, with disruption or alteration in its expression leading
86 to defects in DNA replication and nuclear morphology, and leading to MTOC amplification
87 [26-28]. In a recent study, the authors generated a transgenic parasite line for inducible
88 knockdown where the destabilization domain system was incorporated into MCMBP
89 ($MCMBP^{HADD}$). Using this system, the addition of a molecule called Shield-1 (Shld1) results
90 in wildtype expression of MCMBP, while the absence of Shld1 results in specific MCMBP
91 knockdown. MCMBP deficient parasites were able to undergo DNA replication, but showed
92 severe microtubule defects and aneuploidy; attributed to defective DNA segregation [25].
93 Importantly, while this work was performed with state-of-the-art Airyscan microscopy at the
94 time of publication, they were unable to visualize several important facets of mitosis and
95 microtubules in MCMBP-deficient parasites due to the resolution limit of this techniques.
96 Notably, the limited resolution meant it could not be determined whether aberrant microtubules
97 represented hemispindles or interpolar spindles. Additionally, the absence of a nuclear
98 envelope marker meant that it could not be determined whether microtubule structures were
99 present in the shared, or separate, nuclei.

100 Here, we use U-ExM to study spatial organization of intranuclear microtubules and nuclear
101 division in the context of MCMBP deficient parasites. Additionally, we develop the first U-
102 ExM compatible nuclear envelope stain. We use U-ExM to show that MCMBP deficient
103 parasites display defective hemispindles and mitotic spindles. Additionally, we couple U-ExM

104 and nuclear envelope staining to show that MCMBP deficient parasites form anaphase
105 chromatin bridges, which leads to aneuploidy and the presence of multiple microtubule
106 structures contained within the same nuclear envelope.

107 METHODS

108 ***Plasmodium falciparum* culture**

109 All parasites used in this study were the previously generated transgenic parasite line
110 3D7-PfMCMBP^{3HADD} [25]. For routine culture parasites were grown in O^+ human red blood
111 cells at hematocrit of 4% in RPMI-1640 supplemented with 50 mg/L hypoxanthine, 25 mM
112 HEPES, 0.5% w/v Albumax II and incubated in a mixture of 1% O_2, 5 % CO_2 and 94 % N_2 as
113 previously described [29]. Additionally, to prevent degradation of MCMBP through the
114 destabilization domain system, parasites were cultured in the presence of 250 nM Shield-1 as
115 previously described [25,30].

116 Parasites were tightly synchronized using a combination of Percoll concentration and
117 sorbitol lysis. Briefly, schizont-stage cultures were resuspended in 60 % Percoll and separated
118 from uninfected red blood cells by centrifugation as previously described [31]. Concentrated
119 schizonts were then allowed to reinvade new red blood cells for ~3 hours under normal culture
120 conditions. Following reinvasion, parasite cultures were resuspended in 5% w/v D-sorbitol to
121 selectively lyse schizonts that had not reinvaded, as previously described [32].

122 For assays requiring knockdown of MCMBP, and therefore washout of Shield-1,
123 synchronized schizont-stage cultures (~44-46 h.p.i.) were separated from uninfected red blood
124 cell using QuadroMACS® magnet activated cell sorting [33]. Parasites were allowed to
125 reinvade in the absence of Shield-1 for ~3 hours before being synchronized with sorbitol. As
126 it has been previously shown that knockdown of MCMBP delays parasite growth by

127 approximately three hours [25], parasites grown in the absence of Shield-1 were always
128 collected three hours after those grown in the presence of Shield-1.

129 For assays where segmented schizonts were harvested, schizont-stage cultures (~44
130 h.p.i.) were treated with the schizont egress inhibitor [34] trans-Epoxysuccinyl-L-
131 leucylamido(4-guanidino)butane (E64) at 10 μM for ~5 hours.

132 **Immunofluorescence assays**

133 Immunofluorescence assays in this study were adapted form previously published
134 protocols [17,25]. Briefly, for immunofluorescence assays of unexpanded parasites, ~1 mL of
135 parasite culture at 2% hematocrit was centrifuged at 2,000 rpm in a benchtop centrifuge, the
136 supernatant removed, and the culture resuspended in 4 % w/v paraformaldehyde-PBS before
137 incubating at room temperature for 10 minutes. Fixed parasite cultures were again centrifuged
138 at 2,000 rpm, with the fixative removed and ~3 μL of packed red blood cell pellet smeared
139 onto a glass slide and dried. Dried smears were washed three times in PBS before being
140 permeabilized with 0.1 % v/v Triton-X-100 for 10 minutes at room temperature. Following
141 permabilization, smears were washed three times in PBS and blocked in 3 % w/v bovine serum
142 albumin in PBS for 60 minutes at room temperature. After blocking, smears were incubated
143 with primary antibodies diluted in blocking solution for one hour at room temperature,
144 followed by three washes in PBS. Slides were then incubated with secondary antibodies and
145 NHS ester diluted in PBS for one hour at room temperature. Following antibody staining, slides
146 were washed three times in PBS, dried, mounted with ProLong™ Glass with NucBlue™
147 (ThermoFisher Cat. No. P36981) and a #1.5 coverslip placed on top of the smear.

148 **Ultrastructure Expansion Microscopy**

149 Ultrastructure Expansion Microscopy (U-ExM) was performed as previously described
150 [16,22,35], with significant modification.

151 12 mm round coverslips (Fisher Cat. No. NC1129240) were treated with poly-D-lysine
152 for 1 hour at 37 °C, washed twice with MilliQ water, and placed in the wells of a 12-well plate.
153 Parasite cultures were set to 0.5 % hematocrit, and 1 mL of parasite culture was allowed to
154 settle onto the coverslip for 15 minutes at 37 °C. Culture supernatants were removed, and
155 cultures were fixed with 1 mL of 4% w/v PFA/PBS for 15 minutes at 37 °C. Following fixation,
156 coverslips were washed three times with PBS pre-warmed to 37 °C before being treated with
157 1 mL of 1.4 % v/v formaldehyde / 2% v/v acrylamide (FA/AA) in PBS. After addition of the
158 FA/AA solution, the 12 well plate was parafilmed shut and left to incubate at 37 °C overnight.

159 Monomer solution (19 % w/w sodium acrylate (Sigma Cat. No. 408220), 10% v/v
160 acrylamide (Sigma Cat. No. A4058), 2 % v/v N,N'-methyllenebisacrylamide (Sigma Cat. No.
161 M1533) in PBS) was made in 1 mL batches on Day 1 and stored as 90 µL aliquots at -20 °C
162 overnight.

163 10 % v/v tetraethylenediamine (TEMED; ThermoFisher Cat. No. 17919) and 10 % w/v
164 ammonium persulfate (APS; ThermoFisher Cat. No. 17874) aliquots were thawed on ice, while
165 a humidity chamber containing parafilm was stored at -20 °C before also being placed on ice.
166 FA/AA solution was removed, coverslips were washed once with PBS, dried, and placed cell-
167 side up on the parafilm in the humidity chamber. 5 µL of both TEMED and APS were added
168 per 90 µL of monomer solution, which was briefly vortexed, and 35 µL pipetted onto the
169 parafilm before the coverslip was placed cell-side down onto the monomer solution. Gels were
170 then incubated at 37 °C for 1 hour before being transferred into the wells of a 6-well plate filled
171 with denaturation buffer for 15 minutes at room temperature (200 mM sodium dodecyl sulfate

172 (SDS), 200 mM NaCl, 50 mM Tris, pH 9). Gels were then separated from coverslips and
173 transferred into Eppendorf tubes containing denaturation buffer and denatured at 95 °C for 90
174 minutes. Denatured gels were transferred into 10 cm Petri dishes filled with 25 mL MilliQ
175 water and placed on platform shaker for 30 minutes, with the water replaced twice, each for a
176 further 30 minutes. After the first expansion in water, expanded gels were shrunk by adding 25
177 mL two PBS washes each for 15 minutes. Shrunken gels were placed into the wells of a 6-well
178 plate filled with blocking buffer (3% BSA-PBS) and blocked for 1 hour at room temperature
179 on a platform shaker. After blocking, primary antibodies were prepared in 1 mL of blocking
180 buffer and gels were incubated with primary antibody overnight at room temperature on a
181 platform shaker.

182 Gels were washed three times in 0.5 % v/v PBS-Tween 20 (PBS-T), each for 10
183 minutes, before being incubated with 1 mL of secondary antibodies, NHS ester and/or nuclear
184 stain diluted in PBS for 2.5 hours at room temperature on a platform shaker. Following
185 secondary incubation, gels were washed three times in PBS-T. Stained gels were then
186 transferred back to 10 cm Petri dishes and underwent a second round of expansion with three
187 30 minutes washes in 25 mL MilliQ water.

188 The diameter of fully expanded gels was measured using a tape measure and the
189 expansion factor determined by dividing the expanded gel size (in mm) by the initial coverslip
190 size (12mm). Gel diameter and expansion factor for all gels prepared in this study can be found
191 Supplementary Figure 1.

192 For gels stained with BODIPY TR Ceramide (BODIPY TRc), sections of the expanded
193 gel were cut and placed into the wells of a 6-well plate containing 1 mL 2 μM BODIPY TRc
194 in MilliQ and incubated on a platform shaker overnight.

195 To prepare gels for imaging, small sections were cut from the larger gel and gently dried before
196 being placed into 35 mm #1.5 coverslip bottomed imaging dishes (Cellvis; Fisher Cat. No.
197 NC0409658) that had been pre-coated with poly-D-lysine.

198 **Stains and antibodies**

199 The following primary antibodies were used in this study: Mouse IgG1 anti-alpha
200 Tubulin Clone B-5-1-2; ThermoFisher cat. No. 32-2500 (1:1000 unexpanded samples, 1:500
201 U-ExM samples), Mouse IgG2a anti-Centrin-1 Clone 20H5; EMD Millipore cat. No. 04-1624
202 (1:100 U-ExM samples), Rabbit polyclonal anti-PfBiP; generously provided by Dr. Jeff Dvorin
203 (1:500 U-ExM samples).

204 The following secondary antibodies were used in this study: Goat anti-mouse IgG
205 Alexa Fluor 488 Superclonal™; ThermoFisher Cat. No. A28175 (1:1000 unexpanded samples,
206 1:500 U-ExM samples), Goat anti-mouse IgG2a Alexa Fluor 488 Cross-Adsorbed;
207 ThermoFisher Cat. No. A21131 (1:500 U-ExM samples), Goat anti-mouse IgG1 Alexa Fluor
208 594 Cross-Adsorbed; ThermoFisher Cat. No. A21125 (1:500 U-ExM samples), Goat anti-
209 mouse IgG1 Alexa Fluor 647 Cross-Adsorbed; ThermoFisher Cat. No. A21240 (1:500 U-ExM
210 samples), Goat anti-rabbit Alexa Fluor 488 Highly Cross-Adsorbed; ThermoFisher Cat. No.
211 A11034 (1:500 U-ExM samples).

212 The following stains were used in this study: NucBlue™/Hoechst 33342 (in ProLong
213 Glass™ mountant), DAPI (2 µg/mL U-ExM samples), NHS Ester Atto 594 in DMSO; Sigma
214 Cat. No. 08741 (10 µg/mL unexpanded samples. 10 µg/mL U-ExM samples), NHS Ester Alexa
215 Fluor 405 in DMSO; ThermoFisher Cat. No. A30000 (8 µg/mL U-ExM samples), DRAQ5™;
216 ThermoFisher Cat. No. 62251 (20 µM U-ExM samples), SYTOX™ Deep Red; ThermoFisher
217 Cat. No. S11381 (1 µM U-ExM samples), BODIPY TR Ceramide in DMSO; ThermoFisher
218 Cat. No. D7540 (2 µM U-ExM samples).

219 A comprehensive list of all primary antibodies, secondary antibodies, and stains used
220 for each of the images presented in this study can be found in Supplementary Table 1.

221 **Image acquisition**

222 All microscopy presented in this study was performed on a Zeiss LSM800
223 AxioObserver microscope that had an Airyscan detector. Additionally, all images were
224 acquired using a 63x Plan-Apochromat (NA 1.4) objective lens. All images presented in this
225 study were acquired as Z-stacks with an XY pixel size of 0.035 µm and a Z-step size of 0.15
226 µm. All images then underwent Airyscan processing using ZEN Blue (Version 3.1).

227 **Image analysis**

228 All image analysis performed in this study used ZEN Blue (Version 3.1). All
229 measurements of length were made using the "profile" function of ZEN Blue.

230 To measure hemispindle branch length, maximum intensity projections were made of
231 Airyscan-processed images. Hemispindle branches were first counted and then were measured
232 from the edge of the tubulin staining closest to the MTOC (visible on the NHS Ester channel)
233 to the edge of the tubulin staining furthest away from the MTOC. Nuclei that contained both
234 hemispindles and interpolar spindles were excluded from this analysis. In nuclei that contained
235 multiple MTOCs, it could not always be determined which MTOC each branch was coming
236 from, and so these nuclei were excluded from this analysis.

237 To measure mitotic spindle length, maximum intensity projections were made of
238 Airyscan-processed images. Mitotic spindle size was measured as the greatest distance between
239 the edge of the tubulin staining that was adjacent to each of the two MTOCs.

240 **Statistical analyses**

241 This study reports both the measured distances of mitotic and hemispindles, and then
242 estimated actual distances in unexpanded parasites. To estimate actual distances, the mean
243 expansion factor of all gels used in this study was determined (4.3x; Supplementary Figure 1c).
244 All actual distances were then divided by this mean expansion factor to get the actual estimated
245 distances reported in this study.

246 All graphs and statistical analyses in this study were performed and generated using
247 GraphPad PRISM 9. All values of statistical significance in this study were determined using
248 an unpaired, two-tailed T-test.

249 RESULTS

250 **Ultrastructure expansion microscopy (U-ExM) significantly enhances visualization of**
251 **microtubule structures in *P. falciparum***

252 To validate the utility of U-ExM for visualizing microtubules in *P. falciparum*, we first
253 confirmed that we could visualize all previously identified microtubule structures
254 (hemispindle, mitotic spindle, interpolar spindle, subpellicular microtubules) in unexpanded
255 parasites (Figure 1a). Additionally, we incorporated a general protein stain (N-
256 hydroxysuccinimide (NHS) ester). In unexpanded parasites, NHS ester staining did not
257 produce a distinct or recognizable staining pattern. Despite this, NHS ester staining appeared
258 denser around the likely position of the microtubule organizing center (MTOC) prior to
259 segmentation (Figure 1a). Additionally, NHS ester staining appeared denser at the apical tip of
260 merozoites in segmented schizonts, reminiscent of staining previously observed for the double-
261 bulbous rhoptries [36,37] (Figure 1a).

262 Despite its unclear staining in unexpanded parasites, U-ExM parasites stained with
263 NHS ester allowed the clear and striking identification of many intracellular structures.
264 Through differences in staining intensity, the location of the red blood cell (RBC) membrane,
265 parasite vacuole membrane (PVM) and parasite plasma membrane (PPM) could all be inferred
266 (Figure 1b). Prior to segmentation, the MTOC can be clearly identified based on NHS staining,
267 and it roughly adopts a 'bell-shape' with the most intense NHS ester staining at the top of the
268 bell, and least at the bottom. Additionally, comparing NHS ester staining and chromatin
269 staining it can be seen that there is a density of NHS ester on the nuclear side of the MTOC
270 that does not contain chromatin; which likely represents a recently identified chromatin-free
271 nuclear compartment adjacent to the MTOC [16]. In fully segmented schizonts, the MTOC is
272 no longer visible by NHS ester staining but instead we see the characteristic double-club-
273 shaped rhoptries stained prominently (Figure 1b). At the apex of the rhoptry neck a ring
274 structure can be observed (Figure 1b), which is likely the apical polar rings as it attaches to the
275 subpellicular microtubules at the apical end of the parasite. At the basal end of the parasite, the
276 subpellicular microtubules connect to another ring by NHS ester staining that is likely the basal
277 complex (Figure 1b). Notably, microtubule structures themselves were never observed with
278 NHS ester staining alone.

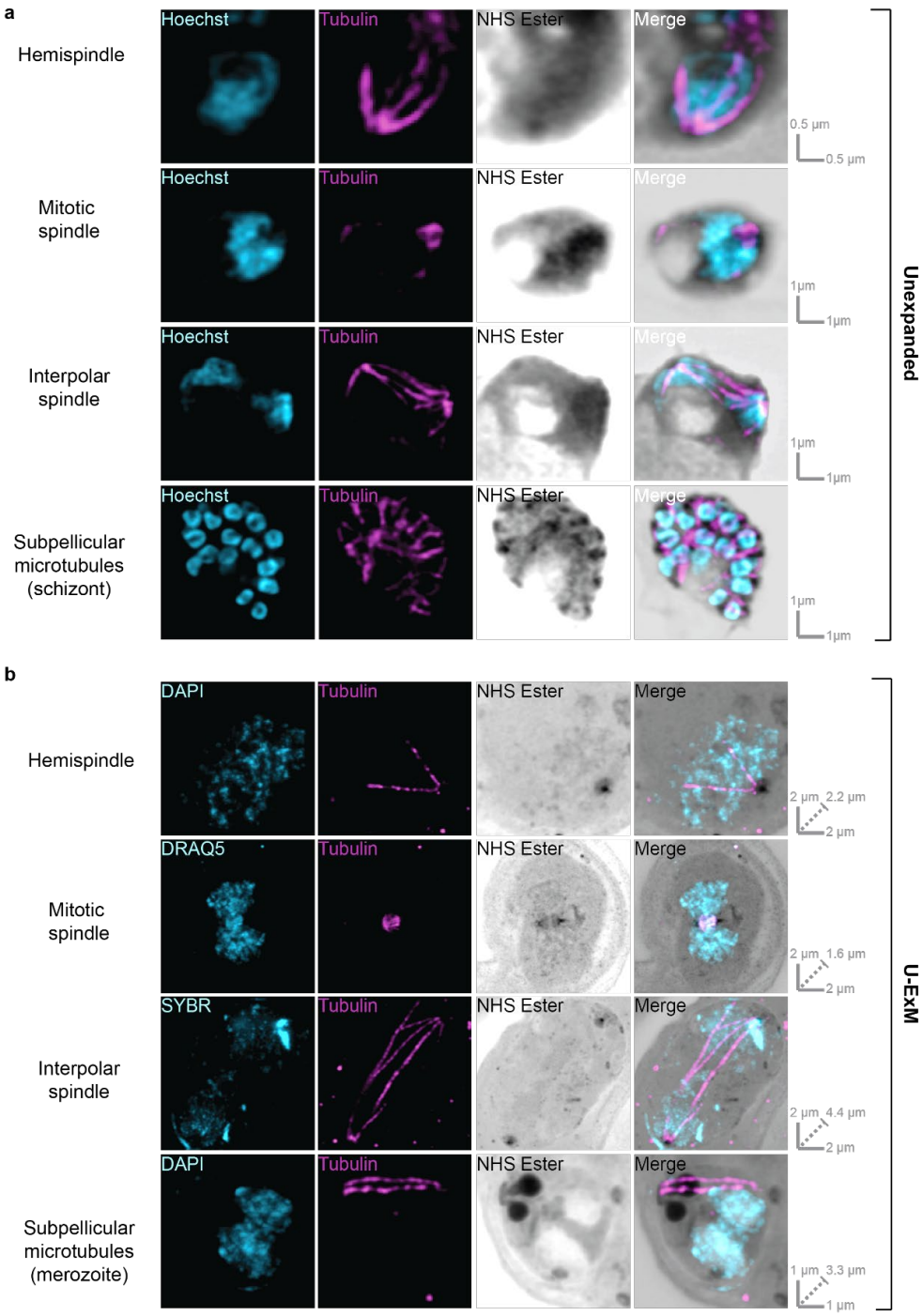

279

280 **Figure 1: Comparison between microtubule structures visualized in unexpanded and U-ExM *P.***
281 ***falciparum* asexual blood-stage parasites.**
282 *MCMBP^{HADD} parasites, cultured in the presence of Shld1, were imaged using super-resolution Airyscan*
283 *microscopy after being prepared for regular immunofluorescence assay* ***(a)****, or U-ExM* ***(b)****. All parasites were*
284 *stained with a nuclear stain (Hoechst, DAPI, DRAQ5, or SYBR in cyan), anti-tubulin (in magenta) and a protein*
285 *stain (N-hydroxysuccinimide (NHS) Ester in greyscale). All previously identified blood-stage microtubule*
286 *structures (hemispindle, mitotic spindle, interpolar spindle and subpellicular microtubules) were observed by*
287 *both IFA and U-ExM. Images in* ***(a)*** *represent a single z-slice from a z-stack image, while images in* ***(b)*** *are*
288 *maximum-intensity projections. Slice-by-slice videos of images in 1b found in Supplementary Videos 1-4. Scale*
289 *bars as labelled in each image, solid bars = XY scale, dashed bar = combined depth of slices used for Z-*
290 *projection.*

291 All microtubule structures were also observed following U-ExM but could be observed
292 in far greater detail with less confounding complexity from neighboring nuclei (Figure 1b).
293 Notably, all the branches of a hemispindle could be readily differentiated including many small
294 branches that previously would have been below the limit of detection (Figure 1b, Figure
295 2a&b). In mitotic spindles both sides of the spindle, connected to either MTOC, could be
296 differentiated and the individual branches that would connect to the kinetochore during mitosis
297 could be observed (Figure 1b). Interpolar spindles were observed connecting two distant
298 MTOCs (Figure 1b). Additionally, these interpolar spindles were found alongside microtubules
299 that extended most of the way to the other MTOC but not completely, and branches that
300 resembled those in a hemispindle (Figure 1b). In merozoites from segmented schizonts,
301 subpellicular microtubules were observed, with typically 2-4 individual microtubules in each
302 merozoite (Figure 1b). Collectively, this shows that U-ExM, coupled with NHS ester staining,
303 can be used to visualize *P. falciparum* microtubules at a single-nucleus level.

304 **MCMBP deficient parasites display aberrant hemispindles and mitotic spindles.**

305 It has previously been observed that MCMBP deficient parasites display microtubule
306 defects [25], but due to the resolution limit of conventional light microscopy prevented
307 exploration of the nature of these defects. Given that each of the microtubule structures could
308 be distinguished from each other using U-ExM (Figure 1b), we used this technique to study
309 microtubule formation in MCMBP deficient parasites.

310 $MCMBP^{HADD}$ parasites either in the presence or absence of Shld1 were stained with
311 antibodies against tubulin and centrin, a nuclear stain, and NHS ester. All images were acquired
312 using Airyscan microscopy after U-ExM. In both hemispindles and mitotic spindles, centrin
313 staining colocalized with the previously described 'bell-shape' of the MTOC observed on NHS
314 ester staining (Figure 2a&e). Notably, however, centrin staining did not colocalize with the

315 entirety of the MTOC, with centrin foci contained within a small portion of the whole MTOC.
316 By comparing with the nuclear stain, it could be seen that centrin foci localized towards the
317 cytoplasmic side of the MTOC structure, suggesting that *P. falciparum* may compartmentalize
318 subsets of proteins inside the MTOC.

319 In MCMBP deficient parasites, MTOC staining often appeared aberrant with misplaced
320 centrin foci (Figure 2e). However, these defects were not consistent or easily quantifiable by
321 regular microscopy measurement techniques. The nature of these defects is unclear but suggest
322 that MCMBP knockdown may alter the formation or integrity of the MTOC.

323 In the presence of Shld1 (Figure 2a), hemispindle branches were on average 732 nm in
324 length (±498 nm SD) (Figure 2b), with the longest branch in each hemispindle being 1260 nm
325 (±512 nm SD) (Figure 2c), and each hemispindle containing 5 branches (±2.2 SD) (Figure 2d).
326 In the absence of Shld1 (Figure 2a), hemispindle branches were on average 31.4 % longer
327 (1067 nm ±815 nm SD) (Figure 2b), with the longest branch in each hemispindle being 32.5
328 % longer (1866 nm ±936 nm SD) (Figure 2c), and each hemispindle containing 18.3 % more
329 branches (6.2 branches ±2.8 SD) (Figure 2d). This suggests that control of hemispindle branch
330 length and number is altered in MCMBP deficient parasites.

331 Mitotic spindles from parasites cultures either in the presence or absence of Shld1 were
332 also imaged and measured (Figure 2e). In the presence of Shld1, mitotic spindles form in an
333 orderly fashion with branches that extend from each of the MTOC towards the opposing
334 MTOC and meet near the middle. By contrast, in the absence of Shld1, branches from the
335 mitotic spindle appeared more heterogeneous in length, but do not appear to extend towards
336 the other MTOC or meet near the middle of the two MTOCs. Moreover, mitotic spindles were
337 23% larger in the absence of Shld1 (691 nm ± 202 nm SD) than in the presence of Shld1 (529
338 nm ± 76 nm SD) (Figure 2f). This suggests that MCMBP deficient parasites form larger mitotic
339 spindles, where the organization and positioning of spindle branches is aberrant.

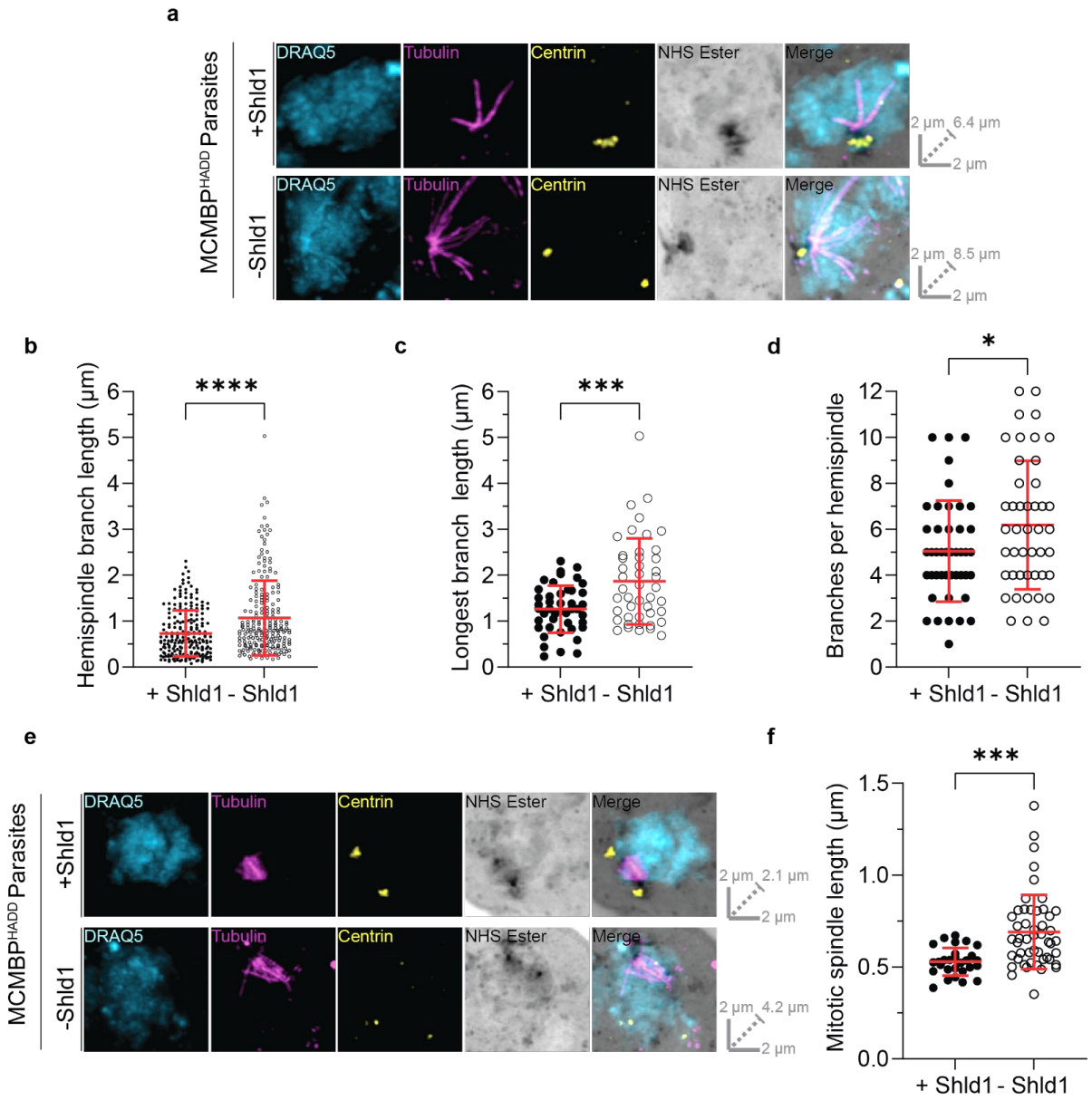

Figure 2. MCMBP deficient parasites show defects in both mitotic spindle and hemispindle formation.

MCMBP^{HADD} parasites were cultured [+]/[-] Shld1. Parasites were then prepared for U-ExM, stained with a nuclear stain (DRAQ5, in cyan), anti-tubulin (in magenta), anti-centrin (in yellow), and a protein stain (NHS Ester, in grayscale), and visualized using Airyscan microscopy. ***(a)*** *Hemispindles were imaged and the length of all hemispindle branches* ***(b)****, of the longest branch in each individual hemispindle* ***(c)****, and the total number of branches per hemispindle* ***(d)*** *were all measured. n = 221 hemispindle branches and 45 hemispindles for +Shld1, and 214 hemispindle branches and 45 hemispindles for -Shld1 were measured across 3 biological replicates.* ***(e)*** *Mitotic spindles were imaged and their length* ***(f)****, from one MTOC to another, was measured. n = 28 for +Shld1 and 49 for -Shld1, across 3 biological replicates. All distance measurements presented here have been estimated based on the average expansion factor of gels used in this study, raw values can be found in Supplementary Figure 2. (* = p < 0.05, *** = p <0.001, **** = p < 0.0001 by unpaired two-tailed t-test, error bars = SD). All images are maximum intensity projections. Slice-by-slice videos of images in found in Supplementary Videos 5-8. Scale bars as labelled in each image, solid bars = XY scale, dashed bar = combined depth of slices used for Z-projection.*

356 **BODIPY TR ceramide stains the nuclear envelope of *P. falciparum* imaged by U-ExM.**

357 *Plasmodium* undergoes mitosis without breakdown of the nuclear envelope, and in
358 doing so the nuclear envelope provides a critical barrier for the compartmentalization of the
359 nucleus from the cytoplasm. Therefore, nuclear envelope integrity and remodeling are critical
360 during *Plasmodium* mitosis. Despite the importance of nuclear envelope dynamics during
361 schizogony, and *Plasmodium* mitosis, there is currently no reliable marker of the *P. falciparum*
362 nuclear envelope for microscopic visualization. Previous studies have localized a few
363 nucleoporins (nups) to the nuclear envelope of either *P. falciparum* [16,38] or *P. berghei* [39],
364 but their distribution and number is dynamic across the lifecycle, limiting the robustness of
365 nups as nuclear envelope markers. Therefore, we wanted to identify a uniform, U-ExM
366 compatible stain for the *P. falciparum* nuclear envelope to allow us to study nuclear envelope
367 changes in the context of MCMBP deficient parasites.

368 BODIPY TR ceramide (BODIPY TRc) is a commonly used fluorescent lipid stain,
369 which has previously been used to stain live parasites from multiple different parasite lifecycle
370 stages, across *P. falciparum* and *P. berghei*, and imaged in both fixed and live-cell microscopy
371 [39-43]. Despite its extensive use, BODIPY TRc has not previously been reported to stain the
372 nuclear envelope of *P. falciparum*. We coupled BODIPY TRc with U-ExM, with BODIPY
373 TRc staining occurring post-expansion. Remarkably, we found that the *P. falciparum* nuclear
374 envelope is consistently and reliably labelled by BODIPY TRc (Figure 3a). In addition to
375 staining the nuclear envelope, BODIPY TRc enabled observation of the RBC membrane,
376 PVM, PPM, and endoplasmic reticulum as previously demonstrated when staining live
377 parasites [42-46] (Supplementary Figure 3). Together, we demonstrate that BODIPY TRc is the
378 first *Plasmodium* nuclear envelope marker enabled by U-ExM.

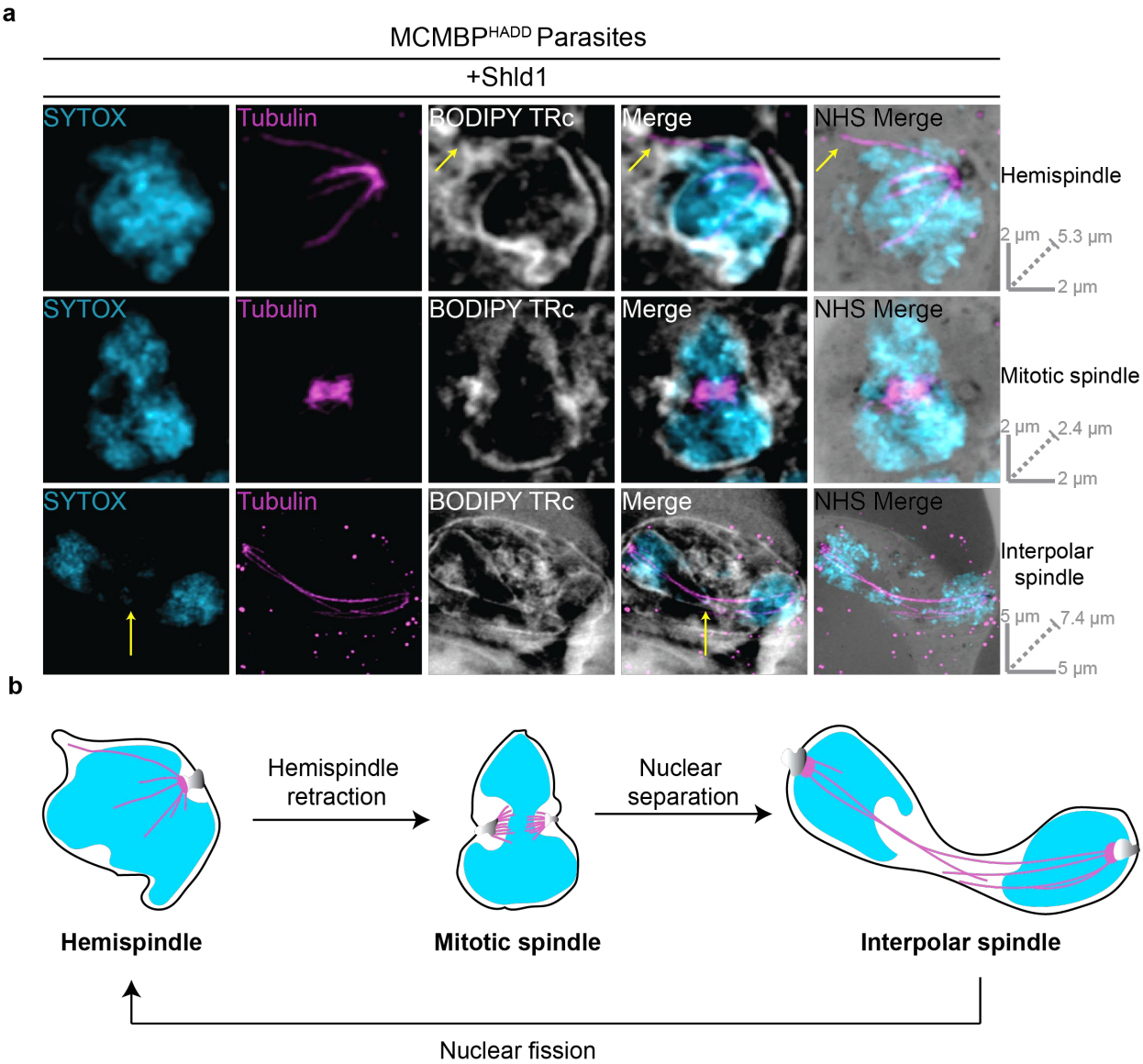

379
380
381 **Figure 3. Nuclear envelope visualized using BODIPY TRc and U-ExM during mitosis of *P.***
382 ***falciparum* blood-stage.**

383 ***(a)*** *MCMBP^HADD parasites were cultured either in the presence) of Shld1. Parasites were then prepared for U-*
384 *ExM, stained with a nuclear stain (SYTOX, in cyan), anti-tubulin (in magenta), a membrane stain (BODIPY Texas*
385 *Red ceramide (TRc), in white), and a protein stain (NHS Ester, in grayscale), and visualized using Airyscan*
386 *microscopy. Hemispindle arrow indicates microtubule not associated with chromatin. Interpolar spindle arrow*
387 *indicates chromatin-free bridge region. Images containing BODIPY TRc are average intensity projections, while*
388 *those with NHS ester are maximum intensity projections. Slice-by-slice videos of images in 3a found in*
389 *Supplementary Videos 9-11. Scale bars as labelled in each image, solid bars = XY scale, dashed bar = combined*
390 *depth of slices used for Z-projection.* ***(b)*** *Model for the progression between observed microtubule structures.*
391 *Hemispindles are first observed but retract before formation of the mitotic spindle once DNA replication has*
392 *occurred. After the formation of the mitotic spindle, two masses of DNA separate from each other but remain in*
393 *a shared nuclear envelope with their MTOCs connected by the interpolar spindle. The nucleus then undergoes*
394 *nuclear fission, separating the two separated DNA masses into daughter nuclei. Following nuclear fission, the*
395 *hemispindle reforms and further rounds of mitosis occur.*

396 To assess the relationship between intranuclear microtubule structures and the nuclear
397 envelop, BODIPY TRc was coupled with U-ExM and tubulin staining (Figure 3a). Nuclei
398 possessing each of the three microtubule structures display differently shaped nuclear
399 envelopes. Nuclei with hemispindles show largely spherical nuclear envelopes, with some
400 notable protrusions of the nuclear envelope to accommodate a hemispindle branch (Figure 3a).
401 Nuclei with mitotic spindles display a marked pinching of the nuclear envelope around the site
402 of the two MTOCs (Figure 3a). Nuclei with interpolar spindles show nuclear envelopes that
403 look characteristically similar to the 'dumbbell-shape' of segregating nuclei in fission yeast
404 (Figure 3a) [24]. Notably, the long and thin bridge region lacks chromatin staining and the
405 interpolar spindles themselves are often present extremely close to the nuclear envelope. By
406 coupling of BODIPY TRc and U-ExM, we refined our model for the progression of
407 intranuclear microtubule structures in *P. falciparum* (Figure 3b).

408 **MCMBP deficient parasites form anaphase chromatin bridges, leading to uneven DNA**
409 **segregation and aneuploidy but still form subpellicular microtubules.**

410 It had previously been observed that MCMBP deficient parasites form complex
411 aberrant spindles and hypothesized that chromatin connected multiple nuclei [25]. In the
412 absence of a nuclear envelope marker, and at the resolution of conventional light microscopy,
413 it could not be determined if these shared a single intact nuclear envelope. By visualizing
414 interpolar spindles of MCMBP-deficient parasites at higher resolution, we were able to update
415 this model. Most prominently, in all interpolar spindles imaged after expansion, there was
416 significant DNA staining inside the bridge region of nuclei connected by interpolar spindles
417 (Figure 4) (Supplementary Figure 4); reminiscent of chromatin bridges that occur during a
418 defective anaphase of other organisms [47,48]. This contrasts with $MCMBP^{HADD}$ parasites
419 grown in the presence of Shld1, where DNA staining was not observed inside this bridge region

420 (Figure 1b,3a). We observed dividing nuclei with interpolar spindles where each nucleus was
421 of vastly different size, potentially indicating uneven DNA segregation (Supplementary Figure
422 4). Moreover, we also observed interpolar spindles connecting MTOCs in nuclei that did not
423 appear to be separating from each other at all (Supplementary Figure 4). Collectively, this
424 suggests that MCMBP deficient parasites can form interpolar spindles but are unable to evenly
425 segregate DNA into daughter nuclei.

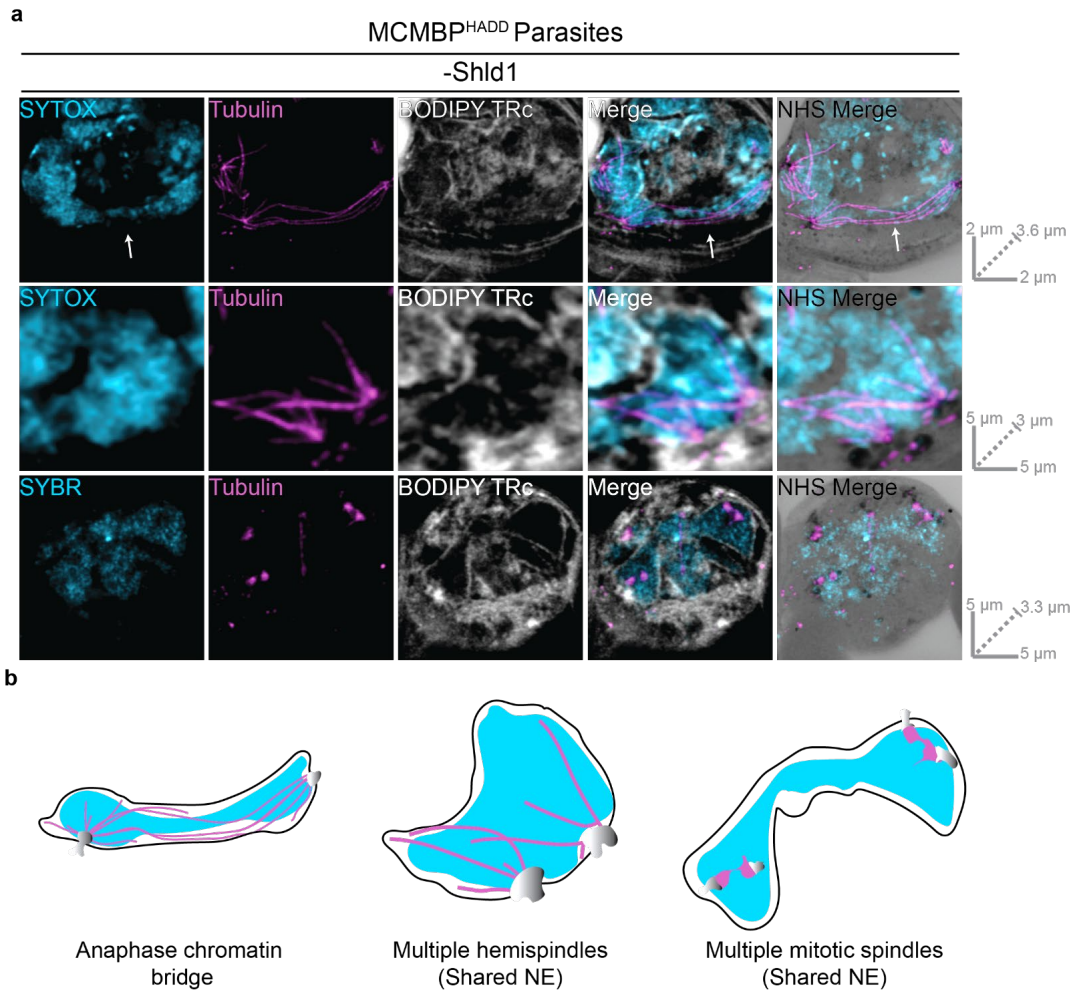

426
427 **Figure 4. MCMBP deficient parasites show defective interpolar spindles, uneven DNA segregation**
428 **and aneuploidy without cell cycle arrest.**

429 ***(a)*** *MCMBP^{HADD} parasites were cultured either in the or absence of Shld1. Parasites were then prepared for U-*
430 *ExM, stained with a nuclear stain (SYTOX or SYBR, in cyan), anti-tubulin (in magenta), a membrane stain*
431 *(BODIPY TRc, in white), and a protein stain (NHS Ester, in grayscale), and visualized using Airyscan microscopy.*
432 *Arrow indicates DNA staining in bridge-region. Images containing BODIPY TRc are average intensity*
433 *projections, while those with NHS ester are maximum intensity projections. Slice-by-slice videos of images in 4a*
434 *found in Supplementary Videos 12-14. Scale bars as labelled in each image, solid bars = XY scale, dashed bar =*
435 *combined depth of slices used for Z-projection.* ***(b)*** *Schematic representation of phenotypes overserved in Figure*
436 *4a.*

437 In MCMBP^{HADD} parasites grown in the absence of Shld1, we also frequently observed
438 a single nuclear envelope that contained multiple microtubule structures and multiple MTOCs
439 not connected by an interpolar spindle (Supplementary Figure 4). Nuclei were observed that
440 contained two hemispindles and two MTOCs, which likely represent nuclei where nuclear
441 fission either did not occur or had occurred aberrantly (Figure 4) (Supplementary Figure 4).
442 Additionally, nuclei that contained two mitotic spindles and four MTOCs were also observed
443 (Figure 4). This suggests that in the aberrant nuclei that contain two MTOCs after mitosis, both
444 MTOCs can duplicate and form mitotic spindles in the same nucleus. Collectively, these
445 observations suggest that MCMBP deficient parasites undergo uneven DNA segregation,
446 leading to aneuploidy and nuclear fission defects, but that these defects don't inhibit further
447 rounds of mitosis as shown previously [25].

448 Following multiple rounds of mitosis, *P. falciparum* commits to segmentation whereby
449 nuclei and other organelles are enclosed into an individual PPM to form merozoites. In
450 segmented merozoites, the MTOC is no longer visible by NHS ester staining and there are no
451 visible intranuclear microtubule structures (Figure 1b). During segmentation, the only visible
452 microtubules are the subpellicular microtubules, which extend from apical polar ring 2 at the
453 apical end of the merozoite to the basal complex as segmentation progresses (Figure 1b) [12,49-
454 51]. MCMBP is not expressed while parasites are undergoing segmentation [25], but
455 considering that MCMBP deficient parasites show intranuclear microtubule defects (Figure 2)
456 (Figure 4) (Supplementary Figure 4), it could be hypothesized that MCMBP knockdown causes
457 downstream subpellicular microtubule defects. To determine whether MCMBP knockdown
458 caused global microtubule defects, or only of the intranuclear microtubules, we analyzed
459 MCMBP^{HADD} parasites grown in the presence of absence of Shld1 that had been arrested post-
460 segmentation with the schizont egress inhibitor E64 [34] by U-ExM.

461 In merozoites from MCMBP^{HADD} schizonts grown in the absence of Shld1 subpellicular
462 microtubules were observed (Supplementary Figure 5), suggesting that MCMBP deficient
463 parasites do not display a global microtubule polymerization defect. However, through NHS
464 ester and BODIPY TRc staining, it was observed that some merozoites contained multiple sets
465 of subpellicular microtubules (Supplementary Figure 5). Additionally, merozoites had vastly
466 differently sized nuclei and contained different varying numbers of rhoptries (Supplementary
467 Figure 5). This confirmed previous observations that merozoites from segmented MCMBP
468 deficient schizonts displayed aneuploidy [25]. Additionally, zoid merozoites, which lack DNA,
469 were observed and they too contained subpellicular microtubules.

470 Collectively, these results show that MCMBP deficient parasites form anaphase
471 chromatin bridges and fail to undergo correct nuclear fission, resulting in aneuploidy and the
472 presence of multiple microtubule structures inside the same nucleus (Figure 5). Despite these
473 severe nuclear defects, these parasites undergo further rounds of mitosis and still undergo
474 segmentation and form subpellicular microtubules; suggesting that MCMBP knockdown
475 doesn't cause global microtubule polymerization defects (Figure 5).

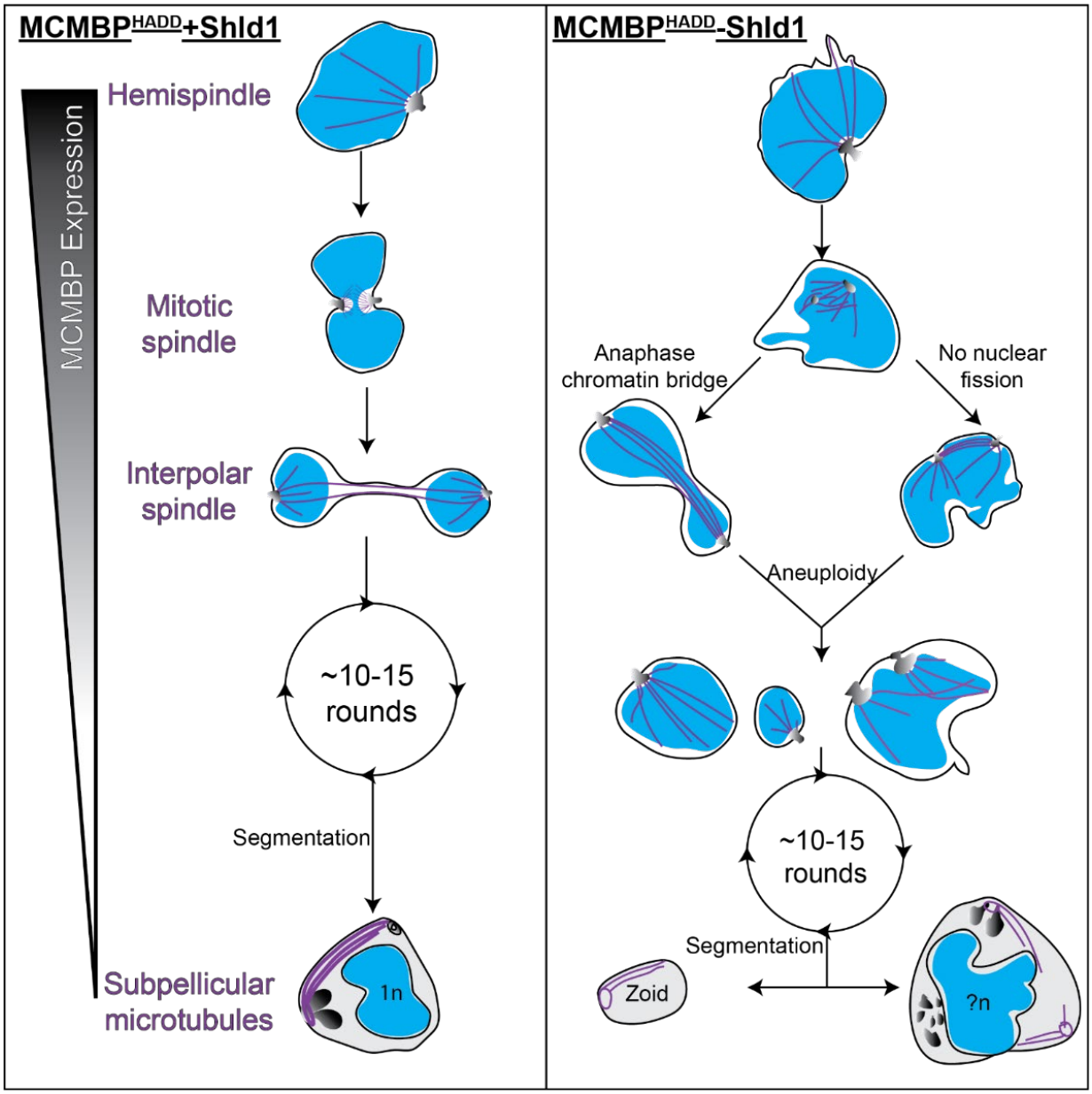

Figure 5. Aneuploidy in MCMBP-deficient parasites is likely caused by the formation of anaphase chromatin bridges and aberrant nuclear fission.
Hypothetical model for the progression of mitosis and segmentation in MCMBP^{HADD} parasites either in the presence (left) or absence (right) of Shld1. In the presence of Shld1, nuclei with a single MTOC form a hemispindle. This hemispindle retracts and the MTOC duplicates and migrates to the opposing side of the nucleus to form the mitotic spindle. The two MTOCs then move away from each other but remain connected by the interpolar spindle. The nucleus then undergoes nuclear fission in the DNA-free bridge region to form two daughter nuclei that each reform a hemispindle. The parasite undergoes multiple rounds of mitosis in this manner. MCMBP is no longer expressed when the parasite commits to segmentation and the formation of merozoites, where we observe subpellicular microtubules connecting the apical polar ring and basal complex. In the absence of Shld1 we observe aberrant hemispindles and mitotic spindles. After forming the mitotic spindle, these nuclei form interpolar spindles, but either form anaphase chromatin bridges and/or fail to undergo nuclear fission, which both lead to aneuploidy. Aneuploid nuclei continue to undergo further rounds of mitosis and do undergo segmentation. Segmentation, however, leads to the formation of cells of various size, including zoid parasites, which lack nuclei, and large merozoites that contain multiple sets of organelles and more than 1n DNA content. Blue = nuclei, purple = microtubules, greyscale = MTOC or rhoptries (in merozoites). n = number of genome copies, ?n = unknown/uneven genome content.

494 DISCUSSION

495 The development of U-ExM and application to *P. falciparum* parasites, have allowed
496 us to understand the functions of proteins and processes of *P. falciparum* to a level of detail
497 not previously possible. We applied U-ExM in the context of MCMBP deficient parasites to
498 significantly refine our understanding of the function of this protein during blood-stage
499 replication of *P. falciparum.*

500 The U-ExM protocol used in this study is largely similar previously published protocols
501 [16,22,35], with the notable modification of changing the protein crosslinking (FA/AA)
502 incubation step from 5 hours to overnight, which significantly shortened day 1 of the U-ExM
503 protocol. In this study, we harvested parasites at multiple timepoints throughout the lifecycle,
504 and all -Shld1 cultures were harvested 3 hours after their +Shld1 counterparts due to the
505 documented growth delay [25]. This shortening of day 1 of the U-ExM protocol made the
506 protocol far more practical, enabling the study of multiple synchronized lifecycle stages
507 without needing to perform independent experiments.

508 In addition to highlighting new biology, our application of U-ExM allowed us to
509 identify some potential drawbacks of this technique. Notably absent in all images of U-ExM
510 parasites were the food vacuole and hemozoin crystal. Through NHS ester staining of
511 unexpanded parasites (Figure 1a), the likely location of the hemozoin crystal and food vacuole
512 could be inferred due to a distinct lack of staining. By contrast, there was no indication on U-
513 ExM parasites of where the hemozoin crystal or food vacuole membrane would be located
514 based on NHS ester or BODIPY TRc staining. We hypothesize that the hemozoin crystal either
515 does not get anchored, or does not expand with the gel, potentially limiting the utility of U-
516 ExM for studies of hemoglobin catabolism and hemozoin biomineralization.

517 In this study a wide range of chromatin stains were used on U-ExM parasites: DAPI,
518 DRAQ5, SYBR Green and SYTOX red. Notably, all these stains showed considerably more
519 photobleaching than we would observe in unexpanded parasites; particularly SYBR Green,
520 which began visibly photobleaching almost immediately. The reason for this is not clear, but
521 it should be noted that while in unexpanded MCMBP deficient parasites a clear nuclear staining
522 defect was observed [25], the same could not be readily observed in U-ExM parasites. At the
523 concentrations used in this study, we found SYTOX red to be the brightest and most
524 photostable of the chromatin stains used. Potentially related to the changes in chromatin was
525 our inability to localize MCMBP by U-ExM. MCMBP has previously been localized in
526 unexpanded parasites, showing nuclear and cytoplasmic foci [25]. Despite this, our attempts to
527 localize MCMBP by U-ExM showed no significant signal. It has been noted previously that
528 some antibodies appear to be incompatible with U-ExM [35], although the reasons for this are
529 unclear, but this does not appear to be the case as the anti-HA antibody we used to detect
530 MCMBP has previously been used successfully on U-ExM samples [16]. Given that the
531 canonical role of MCMBP is to bind DNA, and we observe significant differences in the
532 appearance of DNA in U-ExM parasites, it is possible that some DNA-binding proteins are not
533 retained after U-ExM.

534 BODIPY TRc stained parasites presented in this study were stained post-expansion.
535 We attempted to stain live cells with BODIPY TRc or include BODIPY TRc with the primary
536 or secondary antibody incubations but this uniformly resulted in extremely faint staining (data
537 no shown). Additionally, we tried to stain parasites with Nile red, which has previously been
538 shown to stain some organelles in unexpanded *P. falciparum* blood-stage parasites [44]; but
539 this was also unsuccessful (data now shown). Overall, this suggests that potentially large
540 differences exist in the fluorescent stains that are compatible with unexpanded *P. falciparum*
541 compared to with U-ExM.

542 BODIPY TRc staining of schizonts allowed visualization of the PPM of each
543 merozoite, the PVM, RBC membrane and nuclear envelope, but did not reveal any structures
544 that could be characteristically identified as the apicoplast or mitochondrion as have been
545 identified by EM studies [12]. Additionally, both the surface and lumen the rhoptries of
546 merozoites stained very strongly with BODIPY TRc, which would support previous
547 observations that the rhoptries contain membranous whorls [50,52]. To date, these membranous
548 whorls have not been observed by light microscopy [53], highlighting the use of U-ExM
549 coupled with BODIPY TRc for studying merozoite physiology.

550 We show that MCMBP knockdown results in the aberrant formation of all intranuclear
551 microtubule structures but not of subpellicular microtubules, which are formed when MCMBP
552 is no longer expressed [25]. Moreover, the combination of NHS ester and BODIPY TRc with
553 U-ExM allowed us to assess the MTOC and nuclear envelope at a level of detail reminiscent
554 of electron microscopy. This also confirmed that the in the blood-stage of *P. falciparum* the
555 MTOC spans the nuclear envelope, as previously reported [16]. The combination of BODIPY
556 TRc and NHS ester staining allowed us to show that aneuploidy in MCMBP deficient parasites
557 is due formation of anaphase chromatin bridges and/or a lack of nuclear fission (Figure 5). We
558 hypothesize that these lead to the downstream phenotypes we see of wildly varied nuclear size
559 and zoid merozoites following cytokinesis.

560 The observation of anaphase chromatin bridges in MCMBP-deficient parasites is
561 supported by the canonical function in the MCM complex [26]. In other organisms, the
562 presence of MCMBP has been shown to promote dissociation between the MCM complex and
563 chromatin, allowing separation of sister chromatids [54-56]. Moreover, MCMBP of *P.*
564 *falciparum* has been shown to interact with the members of the condensin complex structural
565 maintenance of chromosomes (SMC) 2 and 4 [25]. SMC2 and SMC4 have canonical roles in
566 chromosome condensation [57,58], and have recently been shown to be involved in *Plasmodium*

567 chromosome separation [59]. Inhibition of SMC2 [60], SMC4 [61] and MCM complex member
568 MCM7 [62] have all been shown to lead to the formation of anaphase chromatin bridges in
569 other organisms. Therefore, we suggest that the observation of anaphase chromatin bridges in
570 MCMBP-deficient *P. falciparum* may be caused by either an ability to properly separate sister
571 chromatids, or a defect in the detachment of microtubules from chromosomes. Currently, the
572 relationship between the formation of anaphase chromatin bridges and nuclear fission is
573 unclear. But given that inhibition of SMC2, SMC4, and MCM7 causes anaphase chromatin
574 bridges in organisms that undergo open mitosis, and therefore do not undergo nuclear fission,
575 defective nuclear fission is not a pre-requisite for the formation of anaphase chromatin bridges.

576 While we observe anaphase chromatin bridges and multiple microtubule structures in
577 a single nucleus following depletion of MCMBP, using $MCMBP^{HADD}$ parasites these events
578 do not occur in every round of mitosis. If this were the case, we would expect to see all
579 chromatin staining contained within a single, giant, nuclear envelope, but we do not. Given
580 that the knockdown system used leads to imperfect and uneven depletion of MCMBP, it is
581 possible that the phenotypic heterogeneity we observe is a product of differing levels of
582 MCMBP. MCMBP is likely essential for growth in the blood-stage of *Plasmodium* [63,64], and
583 we hypothesize that the complete removal of MCMBP would lead to the formation of anaphase
584 chromatin bridges and inhibited nuclear fission in every round of mitosis.

585 Our observations of microtubules, following U-ExM, were largely concordant with
586 recent studies that also made measurements of branch and spindle lengths [16,22].
587 Measurements for mitotic spindle length, hemispindle branch length and hemispindle branch
588 number all reported similar results [16,22]. Neither data set, however, controlled for the
589 number of nuclei per cell and so it is currently unclear whether any of these measurements
590 change later in the parasite lifecycle. One difference observed in our study however, was the
591 presence of hemispindle-like branches in nuclei connected by interpolar spindles (referred to

592 as anaphase spindles in that study) [16]. Previous images have only observed the long
593 interpolar branches connecting the MTOCs, without smaller branches in each nucleus [16].
594 Critically, a previous hypothesis suggested that the hemispindle formed as a remnant of the
595 retraction of the interpolar spindle [65]. Our observation that the two seem to co-exist would
596 suggest that this is not the case. Moreover, this suggests that whatever the function(s) of
597 hemispindles are, likely begin immediately following nuclear segregation and before nuclear
598 fission.

599 Overall, this study provides insight into the poorly understood, yet therapeutically
600 attractive and biologically fascinating, process of mitosis in *P. falciparum.* Our findings
601 significantly further our understanding of the phenotype of parasites following knockdown of
602 MCMBP. Importantly, these insights were only possible because of the application of U-ExM
603 to *P. falciparum*. Moreover, we developed BODIPY TRc as the first U-ExM-compatible stain
604 to visualize the nuclear envelope and used this to develop our understanding of both MCMBP
605 deficient parasites, and parasite physiology more broadly.

606 ACKNOWLEDGEMENTS

607 We thank Jeff Dvorin for provision of anti-BIP antibodies. We thank Julien Guizetti,
608 Eloïse Bertiaux, Vincent Louvel, Caroline Simon, and Johanna Bauer for their help with U-
609 ExM setup. We also thank Julien Guizetti for help with sample preparation when imaging
610 microtubules. We thank Rachel Rudlaff and James Blauwkamp for critical reading of the
611 manuscript.

612

613

AUTHOR CONTRIBUTIONS

Conceptualization, B.L. and S.A.; methodology, B.L.; formal analysis, B.L.; writing—original draft preparation, B.L.; writing—review and editing, B.L. and S.A.; supervision, S.A.; project administration, S.A.; funding acquisition, S.A. All authors have read and agreed to the published version of the manuscript.

FUNDING

This project was supported by an award from the Ralph W. and Grace M. Showalter Research Trust and the Indiana University School of Medicine. The content is solely the responsibility of the authors and does not necessarily represent the official views of the Showalter Research Trust or the Indiana University School of Medicine.

COMPETING INTERESTS

The authors declare no conflict of interest. The funders had no role in the design of the study; in the collection, analyses, or interpretation of data; in the writing of the manuscript, or in the decision to publish the results.

REFERENCES

1. World_Health_Organization. *World Malaria Report 2020*; 2020.

2. Imwong, M.; Dhorda, M.; Myo Tun, K.; Thu, A.M.; Phyo, A.P.; Proux, S.; Suwannasin, K.; Kunasol, C.; Srisutham, S.; Duanguppama, J.; et al. Molecular epidemiology of resistance to antimalarial drugs in the Greater Mekong subregion: an observational study. *The Lancet Infectious Diseases* **2020**, *20*, 1470-1480, doi:https://doi.org/10.1016/S1473-3099(20)30228-0.

635 3. Menard, D.; Dondorp, A. Antimalarial Drug Resistance: A Threat to Malaria
636 Elimination. *Cold Spring Harbor Perspectives in Medicine* **2017**, *7*,
637 doi:10.1101/cshperspect.a025619.

638 4. Ashley, E.A.; Dhorda, M.; Fairhurst, R.M.; Amaratunga, C.; Lim, P.; Suon, S.; Sreng,
639 S.; Anderson, J.M.; Mao, S.; Sam, B.; et al. Spread of artemisinin resistance in
640 *Plasmodium falciparum* malaria. *N Engl J Med* **2014**, *371*, 411-423,
641 doi:10.1056/NEJMoa1314981.

642 5. Uwimana, A.; Legrand, E.; Stokes, B.H.; Ndikumana, J.M.; Warsame, M.; Umulisa,
643 N.; Ngamije, D.; Munyaneza, T.; Mazarati, J.B.; Munguti, K.; et al. Emergence and
644 clonal expansion of *in vitro* artemisinin-resistant *Plasmodium falciparum* kelch13
645 R561H mutant parasites in Rwanda. *Nat Med* **2020**, *26*, 1602-1608,
646 doi:10.1038/s41591-020-1005-2.

647 6. Balikagala, B.; Fukuda, N.; Ikeda, M.; Katuro, O.T.; Tachibana, S.-I.; Yamauchi, M.;
648 Opio, W.; Emoto, S.; Anywar, D.A.; Kimura, E.; et al. Evidence of Artemisinin-
649 Resistant Malaria in Africa. *New England Journal of Medicine* **2021**, *385*, 1163-1171,
650 doi:10.1056/NEJMoa2101746.

651 7. Pham, T.D.M.; Ziora, Z.M.; Blaskovich, M.A.T. Quinolone antibiotics.
652 *Medchemcomm* **2019**, *10*, 1719-1739, doi:10.1039/c9md00120d.

653 8. Magden, J.; Kääriäinen, L.; Ahola, T. Inhibitors of virus replication: recent
654 developments and prospects. *Appl Microbiol Biotechnol* **2005**, *66*, 612-621,
655 doi:10.1007/s00253-004-1783-3.

656 9. Berdis, A.J. Inhibiting DNA Polymerases as a Therapeutic Intervention against
657 Cancer. *Frontiers in Molecular Biosciences* **2017**, *4*, doi:10.3389/fmolb.2017.00078.

658 10. Belete, T.M. Recent Progress in the Development of New Antimalarial Drugs with
659 Novel Targets. *Drug Des Devel Ther* **2020**, *14*, 3875-3889,
660 doi:10.2147/DDDT.S265602.

661 11. Francia, M.E.; Striepen, B. Cell division in apicomplexan parasites. *Nature Reviews*
662 *Microbiology* **2014**, *12*, 125-136, doi:10.1038/nrmicro3184.

663 12. Rudlaff, R.M.; Kraemer, S.; Marshman, J.; Dvorin, J.D. Three-dimensional
664 ultrastructure of *Plasmodium falciparum* throughout cytokinesis. *PLOS Pathogens*
665 **2020**, *16*, e1008587, doi:10.1371/journal.ppat.1008587.

666 13. Rudlaff, R.M.; Kraemer, S.; Streva, V.A.; Dvorin, J.D. An essential contractile ring
667 protein controls cell division in *Plasmodium falciparum*. *Nature Communications*
668 **2019**, *10*, 2181, doi:10.1038/s41467-019-10214-z.

669 14. Gerald, N.; Mahajan, B.; Kumar, S. Mitosis in the Human Malaria Parasite
670 *Plasmodium falciparum*. *Eukaryotic Cell* **2011**, *10*, 474-482,
671 doi:doi:10.1128/EC.00314-10.

672 15. Read, M.; Sherwin, T.; Holloway, S.P.; Gull, K.; Hyde, J.E. Microtubular
673 organization visualized by immunofluorescence microscopy during erythrocytic
674 schizogony in *Plasmodium falciparum* and investigation of post-translational

675 modifications of parasite tubulin. *Parasitology* **1993**, *106 (Pt 3)*, 223-232,
676 doi:10.1017/s0031182000075041.

677 16. Simon, C.S.; Funaya, C.; Bauer, J.; Voß, Y.; Machado, M.; Penning, A.; Klaschka,
678 D.; Cyrklaff, M.; Kim, J.; Ganter, M.; et al. An extended DNA-free intranuclear
679 compartment organizes centrosomal microtubules in *Plasmodium falciparum*. *Life*
680 *Science Alliance* **2021**, *4*, e202101199, doi:10.26508/lsa.202101199.

681 17. Mehnert, A.-K.; Simon, C.S.; Guizetti, J. Immunofluorescence staining protocol for
682 STED nanoscopy of *Plasmodium*-infected red blood cells. *Molecular and*
683 *Biochemical Parasitology* **2019**, *229*, 47-52,
684 doi:https://doi.org/10.1016/j.molbiopara.2019.02.007.

685 18. Schrével, J.; Asfaux-Foucher, G.; Bafort, J.M. Ultrastructural study of multiple
686 mitoses during sporogony of *Plasmodium b. berghei*. *J Ultrastruct Res* **1977**, *59*, 332-
687 350, doi:10.1016/s0022-5320(77)90043-0.

688 19. Fennell, B.J.; Naughton, J.A.; Dempsey, E.; Bell, A. Cellular and molecular actions of
689 dinitroaniline and phosphorothioamidate herbicides on *Plasmodium falciparum*:
690 tubulin as a specific antimalarial target. *Mol Biochem Parasitol* **2006**, *145*, 226-238,
691 doi:10.1016/j.molbiopara.2005.08.020.

692 20. Fennell, B.J.; Al-shatr, Z.A.; Bell, A. Isotype expression, post-translational
693 modification and stage-dependent production of tubulins in erythrocytic *Plasmodium*
694 *falciparum*. *Int J Parasitol* **2008**, *38*, 527-539, doi:10.1016/j.ijpara.2007.09.005.

695 21. Zeeshan, M.; Pandey, R.; Ferguson, D.J.P.; Tromer, E.C.; Markus, R.; Abel, S.;
696 Brady, D.; Daniel, E.; Limenitakis, R.; Bottrill, A.R.; et al. Real-time dynamics of
697 *Plasmodium* NDC80 reveals unusual modes of chromosome segregation during
698 parasite proliferation. *Journal of Cell Science* **2020**, *134*, doi:10.1242/jcs.245753.

699 22. Bertiaux, E.; Balestra, A.C.; Bournonville, L.; Louvel, V.; Maco, B.; Soldati-Favre,
700 D.; Brochet, M.; Guichard, P.; Hamel, V. Expansion microscopy provides new
701 insights into the cytoskeleton of malaria parasites including the conservation of a
702 conoid. *PLOS Biology* **2021**, *19*, e3001020, doi:10.1371/journal.pbio.3001020.

703 23. Rashpa, R.; Brochet, M. Ultrastructure expansion microscopy of *Plasmodium*
704 gametocytes reveals the molecular architecture of a microtubule organisation centre
705 coordinating mitosis with axoneme assembly. *bioRxiv* **2021**, 2021.2007.2021.453039,
706 doi:10.1101/2021.07.21.453039.

707 24. Dey, G.; Culley, S.; Curran, S.; Schmidt, U.; Henriques, R.; Kukulski, W.; Baum, B.
708 Closed mitosis requires local disassembly of the nuclear envelope. *Nature* **2020**, *585*,
709 119-123, doi:10.1038/s41586-020-2648-3.

710 25. Absalon, S.; Dvorin, J.D. Depletion of the mini-chromosome maintenance complex
711 binding protein allows the progression of cytokinesis despite abnormal karyokinesis
712 during the asexual development of *Plasmodium falciparum*. *Cellular Microbiology*
713 **2021**, *23*, e13284, doi:https://doi.org/10.1111/cmi.13284.

714 26. Quimbaya, M.; Raspé, E.; Denecker, G.; De Craene, B.; Roelandt, R.; Declercq, W.;
715 Sagaert, X.; De Veylder, L.; Berx, G. Deregulation of the replisome factor MCMBP

716 prompts oncogenesis in colorectal carcinomas through chromosomal instability.
717 *Neoplasia* **2014**, *16*, 694-709, doi:10.1016/j.neo.2014.07.011.

718 27. Jagannathan, M.; Sakwe, A.M.; Nguyen, T.; Frappier, L. The MCM-associated
719 protein MCM-BP is important for human nuclear morphology. *J Cell Sci* **2012**, *125*,
720 133-143, doi:10.1242/jcs.089938.

721 28. Kim, H.S.; Park, S.H.; Günzl, A.; Cross, G.A. MCM-BP is required for repression of
722 life-cycle specific genes transcribed by RNA polymerase I in the mammalian
723 infectious form of *Trypanosoma brucei*. *PLoS One* **2013**, *8*, e57001,
724 doi:10.1371/journal.pone.0057001.

725 29. Trager, W.; Jensen, J.B. Human malaria parasites in continuous culture. *Science* **1976**,
726 *193*, 673-675, doi:10.1126/science.781840.

727 30. Armstrong, C.M.; Goldberg, D.E. An FKBP destabilization domain modulates protein
728 levels in *Plasmodium falciparum*. *Nature Methods* **2007**, *4*, 1007-1009,
729 doi:10.1038/nmeth1132.

730 31. Trang, D.T.X.; Huy, N.T.; Kariu, T.; Tajima, K.; Kamei, K. One-step concentration of
731 malarial parasite-infected red blood cells and removal of contaminating white blood
732 cells. *Malar J* **2004**, *3*, 7-7, doi:10.1186/1475-2875-3-7.

733 32. Lambros, C.; Vanderberg, J.P. Synchronization of *Plasmodium falciparum*
734 erythrocytic stages in culture. *J Parasitol* **1979**, *65*, 418-420.

735 33. Ribaut, C.; Berry, A.; Chevalley, S.; Reybier, K.; Morlais, I.; Parzy, D.; Nepveu, F.;
736 Benoit-Vical, F.; Valentin, A. Concentration and purification by magnetic separation
737 of the erythrocytic stages of all human *Plasmodium* species. *Malar J* **2008**, *7*, 45,
738 doi:10.1186/1475-2875-7-45.

739 34. Salmon, B.L.; Oksman, A.; Goldberg, D.E. Malaria parasite exit from the host
740 erythrocyte: A two-step process requiring extraerythrocytic proteolysis. *Proceedings*
741 *of the National Academy of Sciences* **2001**, *98*, 271-276, doi:10.1073/pnas.98.1.271.

742 35. Gambarotto, D.; Hamel, V.; Guichard, P. Ultrastructure expansion microscopy (U-
743 ExM). *Methods Cell Biol* **2021**, *161*, 57-81, doi:10.1016/bs.mcb.2020.05.006.

744 36. Liffner, B.; Frölich, S.; Heinemann, G.K.; Liu, B.; Ralph, S.A.; Dixon, M.W.A.;
745 Gilberger, T.-W.; Wilson, D.W. PfCERLI1 is a conserved rhoptry associated protein
746 essential for *Plasmodium falciparum* merozoite invasion of erythrocytes. *Nature*
747 *communications* **2020**, *11*, 1411-1411, doi:10.1038/s41467-020-15127-w.

748 37. Liffner, B.; Balbin, J.M.; Shami, G.J.; Strauss, J.; Frölich, S.; Heinemann, G.K.;
749 Alder, A.; Wichers, J.S.; Tilley, L.; Dixon, M.W.A.; et al. *Pfcerli2*, a duplicated gene
750 in the malaria parasite *Plasmodium falciparum* essential for invasion of erythrocytes
751 as revealed by phylogenetic and cell biological analysis. *bioRxiv* **2020**,
752 2020.2011.2026.400549, doi:10.1101/2020.11.26.400549.

753 38. Guizetti, J.; Martins, R.M.; Guadagnini, S.; Claes, A.; Scherf, A. Nuclear Pores and
754 Perinuclear Expression Sites of *var* and Ribosomal DNA Genes Correspond to

755 Physically Distinct Regions in *Plasmodium falciparum*. *Eukaryotic Cell* **2013**, *12*,
756 697-702, doi:doi:10.1128/EC.00023-13.

757 39. Kehrer, J.; Kuss, C.; Andres-Pons, A.; Reustle, A.; Dahan, N.; Devos, D.;
758 Kudryashev, M.; Beck, M.; Mair, G.R.; Frischknecht, F. Nuclear Pore Complex
759 Components in the Malaria Parasite *Plasmodium berghei*. *Scientific Reports* **2018**, *8*,
760 11249, doi:10.1038/s41598-018-29590-5.

761 40. Dearnley, M.K.; Yeoman, J.A.; Hanssen, E.; Kenny, S.; Turnbull, L.; Whitchurch,
762 C.B.; Tilley, L.; Dixon, M.W.A. Origin, composition, organization and function of the
763 inner membrane complex of *Plasmodium falciparum* gametocytes. *Journal of Cell*
764 *Science* **2012**, *125*, 2053-2063, doi:10.1242/jcs.099002.

765 41. Grüring, C.; Heiber, A.; Kruse, F.; Ungefehr, J.; Gilberger, T.-W.; Spielmann, T.
766 Development and host cell modifications of *Plasmodium falciparum* blood stages in
767 four dimensions. *Nature Communications* **2011**, *2*, 165, doi:10.1038/ncomms1169.

768 42. Thakur, V.; Asad, M.; Jain, S.; Hossain, M.E.; Gupta, A.; Kaur, I.; Rathore, S.; Ali,
769 S.; Khan, N.J.; Mohmmed, A. Eps15 homology domain containing protein of
770 *Plasmodium falciparum* (PfEHD) associates with endocytosis and vesicular
771 trafficking towards neutral lipid storage site. *Biochimica et Biophysica Acta (BBA) -*
772 *Molecular Cell Research* **2015**, *1853*, 2856-2869,
773 doi:https://doi.org/10.1016/j.bbamcr.2015.08.007.

774 43. Tran, P.N.; Brown, S.H.J.; Mitchell, T.W.; Matuschewski, K.; McMillan, P.J.; Kirk,
775 K.; Dixon, M.W.A.; Maier, A.G. A female gametocyte-specific ABC transporter
776 plays a role in lipid metabolism in the malaria parasite. *Nature Communications* **2014**,
777 *5*, 4773, doi:10.1038/ncomms5773.

778 44. Tran, P.N.; Brown, S.H.J.; Rug, M.; Ridgway, M.C.; Mitchell, T.W.; Maier, A.G.
779 Changes in lipid composition during sexual development of the malaria parasite
780 *Plasmodium falciparum*. *Malar J* **2016**, *15*, 73, doi:10.1186/s12936-016-1130-z.

781 45. Adisa, A.; Rug, M.; Klonis, N.; Foley, M.; Cowman, A.F.; Tilley, L. The Signal
782 Sequence of Exported Protein-1 Directs the Green Fluorescent Protein to the
783 Parasitophorous Vacuole of Transfected Malaria Parasites *. *Journal of Biological*
784 *Chemistry* **2003**, *278*, 6532-6542, doi:10.1074/jbc.M207039200.

785 46. Meibalan, E.; Comunale, M.A.; Lopez, A.M.; Bergman, L.W.; Mehta, A.; Vaidya,
786 A.B.; Burns, J.M. Host Erythrocyte Environment Influences the Localization of
787 Exported Protein 2, an Essential Component of the *Plasmodium* Translocon.
788 *Eukaryotic Cell* **2015**, *14*, 371-384, doi:doi:10.1128/EC.00228-14.

789 47. Finardi, A.; Massari, L.F.; Visintin, R. Anaphase Bridges: Not All Natural Fibers Are
790 Healthy. *Genes* **2020**, *11*, 902.

791 48. Zachos, G. Regulating Cytokinesis. In *Encyclopedia of Cell Biology*, Bradshaw, R.A.,
792 Stahl, P.D., Eds.; Academic Press: Waltham, 2016; pp. 494-503.

793 49. Bannister, L.H.; Hopkins, J.M.; Dluzewski, A.R.; Margos, G.; Williams, I.T.;
794 Blackman, M.J.; Kocken, C.H.; Thomas, A.W.; Mitchell, G.H. *Plasmodium*
795 *falciparum* apical membrane antigen 1 (PfAMA-1) is translocated within micronemes

796 along subpellicular microtubules during merozoite development. *Journal of Cell*
797 *Science* **2003**, *116*, 3825-3834, doi:10.1242/jcs.00665.

798 50. Hanssen, E.; Dekiwadia, C.; Riglar, D.T.; Rug, M.; Lemgruber, L.; Cowman, A.F.;
799 Cyrklaff, M.; Kudryashev, M.; Frischknecht, F.; Baum, J.; et al. Electron tomography
800 of *Plasmodium falciparum* merozoites reveals core cellular events that underpin
801 erythrocyte invasion. *Cellular Microbiology* **2013**, *15*, 1457-1472,
802 doi:https://doi.org/10.1111/cmi.12132.

803 51. Koreny, L.; Zeeshan, M.; Barylyuk, K.; Tromer, E.C.; van Hooff, J.J.E.; Brady, D.;
804 Ke, H.; Chelaghma, S.; Ferguson, D.J.P.; Eme, L.; et al. Molecular characterization of
805 the conoid complex in *Toxoplasma* reveals its conservation in all apicomplexans,
806 including *Plasmodium* species. *PLOS Biology* **2021**, *19*, e3001081,
807 doi:10.1371/journal.pbio.3001081.

808 52. Bannister, L.H.; Mitchell, G.H.; Butcher, G.A.; Dennis, E.D. Lamellar membranes
809 associated with rhoptries in erythrocytic merozoites of *Plasmodium knowlesi*: a clue
810 to the mechanism of invasion. *Parasitology* **1986**, *92*, 291-303,
811 doi:10.1017/S0031182000064064.

812 53. Liffner, B.; Balbin, J.M.; Wichers, J.S.; Gilberger, T.-W.; Wilson, D.W. The Ins and
813 Outs of *Plasmodium* Rhoptries, Focusing on the Cytosolic Side. *Trends in*
814 *Parasitology* **2021**, *37*, 638-650, doi:10.1016/j.pt.2021.03.006.

815 54. Sakwe, A.M.; Nguyen, T.; Athanasopoulos, V.; Shire, K.; Frappier, L. Identification
816 and characterization of a novel component of the human minichromosome
817 maintenance complex. *Mol Cell Biol* **2007**, *27*, 3044-3055, doi:10.1128/mcb.02384-
818 06.

819 55. Nishiyama, A.; Frappier, L.; Méchali, M. MCM-BP regulates unloading of the
820 MCM2-7 helicase in late S phase. *Genes Dev* **2011**, *25*, 165-175,
821 doi:10.1101/gad.614411.

822 56. Takahashi, N.; Quimbaya, M.; Schubert, V.; Lammens, T.; Vandepoele, K.; Schubert,
823 I.; Matsui, M.; Inzé, D.; Berx, G.; De Veylder, L. The MCM-binding protein ETG1
824 aids sister chromatid cohesion required for postreplicative homologous recombination
825 repair. *PLoS Genet* **2010**, *6*, e1000817, doi:10.1371/journal.pgen.1000817.

826 57. Stray, J.E.; Lindsley, J.E. Biochemical analysis of the yeast condensin Smc2/4
827 complex: an ATPase that promotes knotting of circular DNA. *J Biol Chem* **2003**, *278*,
828 26238-26248, doi:10.1074/jbc.M302699200.

829 58. Wang, H.; Liu, Y.; Yuan, J.; Zhang, J.; Han, F. The condensin subunits SMC2 and
830 SMC4 interact for correct condensation and segregation of mitotic maize
831 chromosomes. *Plant J* **2020**, *102*, 467-479, doi:10.1111/tpj.14639.

832 59. Pandey, R.; Abel, S.; Boucher, M.; Wall, R.J.; Zeeshan, M.; Rea, E.; Freville, A.; Lu,
833 X.M.; Brady, D.; Daniel, E.; et al. *Plasmodium* Condensin Core Subunits
834 SMC2/SMC4 Mediate Atypical Mitosis and Are Essential for Parasite Proliferation
835 and Transmission. *Cell Reports* **2020**, *30*, 1883-1897.e1886,
836 doi:https://doi.org/10.1016/j.celrep.2020.01.033.

837 60. Strunnikov, A.V.; Hogan, E.; Koshland, D. SMC2, a *Saccharomyces cerevisiae* gene
838 essential for chromosome segregation and condensation, defines a subgroup within
839 the SMC family. *Genes & Development* **1995**, *9*, 587-599, doi:10.1101/gad.9.5.587.

840 61. Steffensen, S.; Coelho, P.A.; Cobbe, N.; Vass, S.; Costa, M.; Hassan, B.; Prokopenko,
841 S.N.; Bellen, H.; Heck, M.M.S.; Sunkel, C.E. A role for *Drosophila* SMC4 in the
842 resolution of sister chromatids in mitosis. *Current Biology* **2001**, *11*, 295-307,
843 doi:10.1016/S0960-9822(01)00096-3.

844 62. Hong, Y.; Sonneville, R.; Wang, B.; Scheidt, V.; Meier, B.; Woglar, A.; Demetriou,
845 S.; Labib, K.; Jantsch, V.; Gartner, A. LEM-3 is a midbody-tethered DNA nuclease
846 that resolves chromatin bridges during late mitosis. *Nature Communications* **2018**, *9*,
847 728, doi:10.1038/s41467-018-03135-w.

848 63. Zhang, M.; Wang, C.; Otto, T.D.; Oberstaller, J.; Liao, X.; Adapa, S.R.; Udenze, K.;
849 Bronner, I.F.; Casandra, D.; Mayho, M.; et al. Uncovering the essential genes of the
850 human malaria parasite *Plasmodium falciparum* by saturation mutagenesis. *Science*
851 **2018**, *360*, eaap7847, doi:doi:10.1126/science.aap7847.

852 64. Bushell, E.; Gomes, A.R.; Sanderson, T.; Anar, B.; Girling, G.; Herd, C.; Metcalf, T.;
853 Modrzynska, K.; Schwach, F.; Martin, R.E.; et al. Functional Profiling of a
854 *Plasmodium* Genome Reveals an Abundance of Essential Genes. *Cell* **2017**, *170*, 260-
855 272.e268, doi:10.1016/j.cell.2017.06.030.

856 65. Canning, E.U.; Sinden, R.E. The organization of the ookinete and observations on
857 nuclear division in oocysts of *Plasmodium berghei*. *Parasitology* **1973**, *67*, 29-40,
858 doi:10.1017/S0031182000046266.

859

860